

HOSTED BY



Contents lists available at ScienceDirect

Journal of King Saud University – Science

journal homepage: [www.sciencedirect.com](http://www.sciencedirect.com)

Original article

# Numerical simulation of the transition of a Newtonian fluid to a viscoplastic state in a turbulent flow

Maksim A. Pakhomov<sup>a,b</sup>, Uzak K. Zhabbasbayev<sup>b,\*</sup>, Daniyar Zh. Bossinov<sup>b</sup><sup>a</sup> Kutateladze Institute of Thermophysics, Siberian Branch of the Russian Academy of Science, Lavrent'ev Ave., 1, 630090 Novosibirsk, Russia<sup>b</sup> Satbayev University, 050013, Satpaev str, 22a, Almaty, Kazakhstan

## ARTICLE INFO

## Article history:

Received 25 April 2022

Revised 14 December 2022

Accepted 21 December 2022

Available online 28 December 2022

## Keywords:

High-viscosity oil

Non-isothermal flow

Bingham-Schwedoff model

Turbulence

Heat transfer

Reynolds stress model

## ABSTRACT

The non-isothermal turbulent flow and transition to a viscoplastic state of high-viscosity oil with physical and chemical properties depending on fluid temperature is numerically studied. The turbulence of fluid flow in a pipe is described using the Reynolds stress, Reynolds algebraic stress, and two-parameter isotropic models. The simulations show the boundaries of the region of the manifestation of Newtonian behavior and fluid transition to a viscoplastic state. The Reynolds stress model and the algebraic Reynolds stress model show significant anisotropy in the velocity fluctuation profiles of Newtonian and non-Newtonian fluids. The shift of the locus of maximal magnitudes of turbulent pulsations, Reynolds stress, and turbulent kinetic energy towards a flow core region is observed. The height of the zone with a completely stopped fluid is predicted and determined numerically. The appearance of a stagnation zone near the wall causes a significant decrease in wall friction and heat transfer due to a decrease in the environment temperature.

© 2022 The Author(s). Published by Elsevier B.V. on behalf of King Saud University. This is an open access article under the CC BY-NC-ND license (<http://creativecommons.org/licenses/by-nc-nd/4.0/>).

## 1. Introduction

Turbulent flows of waxy crude oil (WCO) with heat transfer with the environment occur in the main oil pipelines. The WCO flow can change from Newtonian state to viscoplastic one when environment temperature is cooled (Chhabra and Richardson, 2011; Souas et al., 2021; Zhumagulov et al., 2002). The material properties of such liquids have a strong nonlinear temperature dependence due to the presence of asphaltenes, paraffins, and resins (Aiyejina et al., 2011; Li et al., 2015). The appearance of yield stress causes the emergence of a “stagnant zone” formation in a near-wall zone, where flow rate fully stops (de Oliveira et al., 2010; Li et al., 2015). Therefore, transportation of high-viscosity oil through pipelines is complicated (Aiyejina et al., 2011; Li et al., 2015). Waxy crude oils at temperatures ( $T \geq 298$  K) are Newtonian fluids (NF). The viscoplastic behavior of a fluid appears by

fluid temperature cooling (Aiyejina et al., 2011; Dai, 2019; Bekibayev et al., 2021, 2022; Zhabbasbayev et al., 2021).

Turbulent mean and fluctuational flow structure of a non-Newtonian fluid (NNF) often studied without heat transfer (Cruz and Pinho, 2003; Gavrilo and Rudyak, 2016b; Iaccarino et al., 2010; Malin, 1997). The experimental studies of such flows are very limited due to the complexity of the measurement methods (Escudier et al., 2009; Peixinho et al., 2005). The laser Doppler anemometry is used for measurements of a viscoelastic shear-thinning fluid (Escudier et al., 2009). The experiments were performed in a duct for a fully-developed flow. Three components of turbulent fluctuations and Reynolds shear stress were measured.

An alternative to this is to conduct mathematical modeling of non-Newtonian fluids. The turbulent flows of such fluids are usually modeled using the Reynolds-averaged Navier-Stokes equations (RANS) approach (Durbin and Pettersson Reif, 2011). In these works, turbulence models of various levels are used:  $k-\varepsilon$  (Cruz and Pinho, 2003; Malin, 1997),  $v2-f$  (Iaccarino et al., 2010). The difficulty arising in the mathematical modeling of such flows is that applied turbulence models are difficult to verify using known experimental benchmarks. The theoretical formula of the wall friction coefficient of turbulent Bingham-Schwedoff (BS) fluids is developed in (Anbarlooei et al., 2017).

Direct numerical simulation (DNS) and large eddy simulation (LES) are the main powerful methods for study of NNF. LES

\* Corresponding author.

E-mail addresses: [pakhomov@ngs.ru](mailto:pakhomov@ngs.ru), [pakhomov@itp.nsc.ru](mailto:pakhomov@itp.nsc.ru) (M.A. Pakhomov), [uzak.zh@mail.ru](mailto:uzak.zh@mail.ru) (U.K. Zhabbasbayev), [dansho.91@mail.ru](mailto:dansho.91@mail.ru) (D. Zh. Bossinov).

Peer review under responsibility of King Saud University.



Production and hosting by Elsevier

<https://doi.org/10.1016/j.jksus.2022.102522>

1018-3647/© 2022 The Author(s). Published by Elsevier B.V. on behalf of King Saud University.

This is an open access article under the CC BY-NC-ND license (<http://creativecommons.org/licenses/by-nc-nd/4.0/>).

(Gnambode et al., 2015) and DNS (Gavrilov and Rudyak, 2016a; Rudman and Blackburn, 2006; Singh et al., 2017) works have been performed to investigate the turbulent power-law and viscoplastic and pseudoplastic non-Newtonian fluids. The results of average and fluctuational longitudinal and transverse velocities, wall friction, and the turbulent kinetic energy at Reynolds numbers, Re, from 5000 to 20,000 were obtained. Note that LES and DNS (Gavrilov and Rudyak, 2016a; Gnambode et al., 2015) only dealt with Buckley-Herschel fluids, and only recent paper (Singh et al., 2017) presents DNS prediction data for fluids with yield stress. A few papers concerned the study of heat transfer in turbulent NNF (Masoudian et al., 2016; Masoumi et al., 2019; Yigit et al., 2020). Turbulent flow studies with a viscoelastic flow of a polymer were investigated (Masoudian et al., 2016; Yigit et al., 2020). The DNS study of velocity and temperature spectra in Rayleigh-Bénard convection was performed in the paper (Yigit et al., 2020). The authors showed that thermal convection weakens with growth of the Rayleigh number. Numerical study of natural convection of Bingham-Schwedoff (BS) fluid between horizontal concentric cylinders was carried out in the paper (Masoumi et al., 2019).

The aim of this paper is numerically simulation of turbulent flow structure and heat transfer by transition of incompressible Newtonian fluid (WCO) to viscoplastic NNF in a pipe. This paper is a continuation of our recent work (Pakhomov and Zhabbasbayev, 2021). The authors studied transition of Newtonian fluid to viscoplastic state when cooling of nonisothermal turbulent flow in tube. The fluid flow turbulence is predicted by two-parameter  $k-\tilde{\varepsilon}$  model (Hwang and Lin, 1998). The papers (Gnambode et al., 2015) and DNS (Gavrilov and Rudyak, 2016a; Rudman and Blackburn, 2006; Singh et al., 2017) show that the anisotropy of velocity fluctuations is noticeably higher than that of a Newtonian fluid. Therefore, the use of isotropic turbulence models in the description of such flows is significantly limited by only obtaining results of the mean flow, while predictions of the turbulent characteristics using this approach have led to significant errors.

In this work, the RSM (Manceau and Hanjalic, 2002) and the explicit algebraic Reynolds stress model (ARSM) (Rokni, 2000; Speziale and Xu, 1996) were used to describe the anisotropy property. The following are the research results of turbulent flow and heat transfer of WCO in a pipe using the RSM and the ARSM.

## 2. Mathematical model

### 2.1. Bingham-Schwedoff rheology model

Waxy crude oil rheology can be modeled as the generalized Newtonian fluids (Vinay et al., 2005; Salehi-Shabestari et al., 2016). The effective (apparent) viscosity of a BS fluid is defined using a rheology model (Barnes, 1999; Beverly and Tanner, 1992; Bingham, 1922). The Bingham-Schwedoff model is the simplest model of viscoplastic non-Newtonian fluids (Barnes, 1999; Bingham, 1922):

$$\mu_{eff} = \begin{cases} \mu_p + \tau_0|\dot{\gamma}|^{-1}, & \text{if } |\tau| > \tau_0 \\ \infty, & \text{if } |\tau| \leq \tau_0 \end{cases} \quad (1)$$

where  $\mu_p$  is plastic viscosity, and  $\tau_0$  is yield shear stress,  $\dot{\gamma} = \sqrt{2S_{ij}S_{ij}} = S^2$  is strain rate,  $S_{ij} = 0.5\left(\frac{\partial u_i}{\partial x_j} + \frac{\partial u_j}{\partial x_i}\right)$  is shear rate tensor. If  $\tau_0 = 0$  then fluid is Newtonian, if  $\tau_0 > 0$  then fluid is BS fluid. We use strain rate tensor  $\dot{\gamma}$  as shear rate (Gavrilov and Rudyak, 2016b).

The singularity of a numerical solution of the Eq. (1) is appeared in zones at  $\tau < \tau_0$ . The singular property of the effective viscosity can be solved by improving the original rheological model

(Barnes, 1999). Effective viscosity can be represented as a smooth function using the approach (Papanastasiou, 1987):

$$\mu_{eff} = \mu_p + \frac{\tau_0[1 - \exp(-m|\dot{\gamma}|)]}{|\dot{\gamma}|} \quad (2)$$

where  $m = 10^3$  (Papanastasiou, 1987). The expression (2) overcomes the calculation difficulties in a Bingham-Schwedoff viscoplastic fluid. Thermal effects in rheological properties are taken into account by dependence of viscosity  $\mu_p(T)$  and yield stress  $\tau_0(T)$  on temperature (Zhabbasbayev et al., 2021; Zhumagulov et al., 2002). These dependencies are based on experimental data.

### 2.2. The set of governing equations for a non-Newtonian turbulent fluid

The system of stationary RANS equations for the flow and heat transfer of an incompressible fluid has the form

$$\nabla \cdot \mathbf{U} = 0 \quad (3)$$

$$\nabla \cdot (\rho \mathbf{U}\mathbf{U}) = -\nabla P + \nabla \cdot (2\mu_{eff}\mathbf{S}) + \nabla \cdot (-\rho\langle \mathbf{u}'\mathbf{u}' \rangle) + \nabla \cdot \langle 2\mu'_{eff}\mathbf{S}' \rangle \quad (4)$$

$$\nabla \cdot (\rho C_p \mathbf{T}\mathbf{U}) = \nabla \cdot (\lambda \nabla T) + \nabla \cdot (-\rho C_p \langle \mathbf{u}'t' \rangle) + \tau : \mathbf{S} \quad (5)$$

Here,  $\mathbf{S}$  is averaged strain rate tensor,  $S = \sqrt{2S_{ij}S_{ij}}$  is modulus of averaged strain rate tensor. The turbulent characteristics  $-\rho\langle \mathbf{u}'\mathbf{u}' \rangle$  and  $-\rho C_p \langle \mathbf{u}'t' \rangle$  was written according to Boussinesq hypothesis. The expression  $\nabla \cdot \langle 2\mu'_{eff}\mathbf{S}' \rangle$  in equation (4) is found according to representation (Gavrilov and Rudyak, 2016b). The last term in equation (5) takes into account the dissipation of kinetic energy and has the form (Vinay et al., 2005). In the recent paper (Pakhomov and Zhabbasbayev, 2021) the system of equations (3)–(5) was solved jointly with  $k-\tilde{\varepsilon}$  model (Hwang and Lin, 1998).

The elliptical relaxation RSM (Manceau and Hanjalic, 2002) considers anisotropy of complex turbulent flows and is computationally more difficult than ARSM. These models give better predictable results than the  $k-\tilde{\varepsilon}$  turbulence isotropic model. The ARSM from (Rokni, 2000) is a version of the well-known explicit Reynolds algebraic stress model (Speziale and Xu, 1996). The Reynolds stress components are derived from a system of partial differential equations, and the system of basic equations of the second-moment closure model of (Manceau and Hanjalic, 2002) is given:

$$\begin{aligned} \nabla \cdot (\rho \mathbf{U}\langle \mathbf{u}'\mathbf{u}' \rangle) &= \rho(P_{ij} + \Phi - \varepsilon) + \nabla \cdot \left[ \rho \frac{C_\mu T_T}{\sigma_k} \langle \mathbf{u}'\mathbf{u}' \rangle \nabla (\langle \mathbf{u}'\mathbf{u}' \rangle) \right] \\ \nabla \cdot (\rho \mathbf{U}\varepsilon) &= \frac{1}{T_t} (C_{\varepsilon 1} P_2 - C_{\varepsilon 2} \varepsilon) + \nabla \cdot \left[ \rho \frac{C_\mu T_T}{\sigma_\varepsilon} \langle \mathbf{u}'\mathbf{u}' \rangle \nabla \varepsilon \right] + \nabla \cdot (\mu \nabla \varepsilon) \\ &\quad + C_{\varepsilon 3} \frac{\mu k}{\varepsilon} \langle \mathbf{u}'\mathbf{u}' \rangle \cdot \nabla^2 \mathbf{U} \cdot \nabla^2 \mathbf{U} \\ \chi - L_T^2 \nabla^2 \chi &= 1/(\varepsilon T_T) \end{aligned} \quad (6)$$

Here,  $P_{ij}$  is the intensity of the energy transfer from the average velocity to the pulsating one;  $P_2 = 0.5P_{kk}$ ,  $T_T$  is the turbulent time macroscale;  $\phi$  is the redistribution term (Manceau and Hanjalic, 2002),  $\varepsilon$  is the dissipation rate.

$$\nabla \cdot (\rho Uk) = \nabla \cdot \left[ \left( \mu + \frac{C_\mu \rho k}{\sigma_k \varepsilon} \right) \nabla k \right] + P_{kk} - \rho \varepsilon$$

$$\nabla \cdot (\rho U \varepsilon) = \nabla \cdot \left[ \left( \mu + \frac{C_\mu \rho k^2}{\sigma_\varepsilon \varepsilon} \right) \nabla \varepsilon \right] + \frac{1}{T_T} (f_{\varepsilon 1} C_{\varepsilon 1} P_{kk} - f_{\varepsilon 2} C_{\varepsilon 2} \rho \varepsilon)$$

$$\rho \langle \mathbf{u}' \mathbf{u}' \rangle = 2\mu_T S_{ij} - \frac{2}{3} k \delta_{ij} + \mu_T T_T C_1 [(S_{ik} \Omega_{jk} + S_{jk} \Omega_{ik}) - C_2 S_{ik} S_{jk}] - \frac{1}{3} S_{kl} S_{kl} \delta_{ij} \tag{7}$$

### 2.3. Boundary conditions

All boundary conditions for a non-isothermal flow are given in details (Pakhomov and Zhapbasbayev, 2021). No-slip conditions are set on the wall surface for fluid velocity. The heat transfer coefficient from fluid flow (WCO) to cold soil through pipe surface is determined by the formula (Zhapbasbayev et al., 2021). The symmetry conditions are set on the pipe axis. The uniform distributions of velocity and temperature are set over the cross-section of pipe in inlet section. At the outlet edge, gradients of all flow and heat transfer parameters in axial direction.

### 3. Numerical realization

The flow sketch is shown in the Fig. 1. Numerical predictions are carried out using the “in-house” code. The system of equations (3)–(7) is solved numerically using the QUICK scheme and the SIMPLER algorithm. The simulations use a non-uniform mesh with refinement close to all walls. The cell closest to the wall is located at  $y_+ = yu/v_w = 0.4$ , where  $y = R - r$  is distance from the wall,  $R$  is pipe radius,  $u_*$  is friction velocity of a Newtonian fluid in the inlet pipe and  $\nu_w$  is kinematic viscosity of a fluid at wall condition. The residual error for the continuity equation, momentum equations, and RSM model is  $10^{-5}$  and for the energy equation the error is  $10^{-7}$ .

The grid convergence test (GCT) is performed on the grids:  $500 \times 40$  (coarse),  $1000 \times 80$  (medium) and  $1500 \times 120$  (fine) (see Fig. 2). The GCT results are presented for the RSM (Manceau and Hanjalic, 2002) (see Fig. 2a) and the ARSM (Rokni, 2000) (see Fig. 2b). The GCT for the  $k-\tilde{\varepsilon}$  model was carried out in (Hwang and Lin, 1998). The Reynolds and Prandtl numbers of the flow are  $Re = U_1 D / \nu_{w1} = 0.82 \times 10^4$  and  $Pr = \mu_{w1} C_{p1} / \lambda_1 = 42$ .

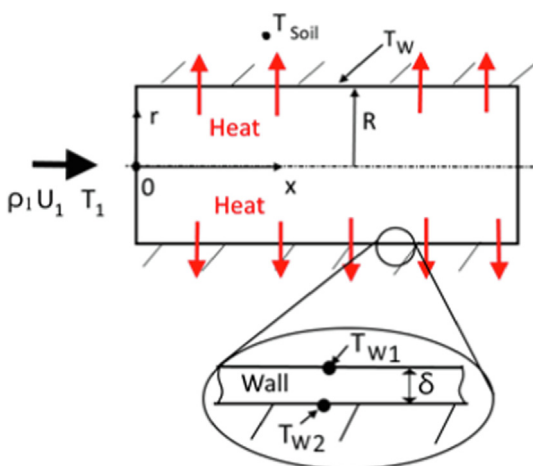


Fig. 1. Flow configuration scheme.

## 4. Results and discussion

### 4.1. Isothermal flow in a pipe

At the first stage, the comparisons with data of DNS predictions for the turbulent flow of Newtonian fluid in pipe were performed. DNS simulations (Singh et al., 2017) on the transverse distributions of axial and radial velocity fluctuations for Newtonian turbulent fluid were used. These results are given in Fig. 3. The maximum differences in the intensity of the axial pulsations of the Newtonian fluid velocity do not exceed 10% when predicted using the RSM model (see Fig. 3a). The largest discrepancy between the data of our numerical RANS simulations and DNS data (Singh et al., 2017) does not exceed 15% and is observed for radial pulsations (see Fig. 3b) at  $y_+ \approx 80$ .

Fig. 4 shows the profiles of (a) axial and (b) radial velocity fluctuations of the Bingham–Schwedoff fluid over the pipe section in the wall units  $y_+$ . The dots are the DNS data (Singh et al., 2017), the lines are the authors’ RANS predictions. The solid lines are the  $k-\tilde{\varepsilon}$  model (Hwang and Lin, 1998), the dashed lines are the RSM model (Manceau and Hanjalic, 2002) and the dotted lines are the full explicit ARSM (Rokni, 2000). In the calculations of the  $k-\tilde{\varepsilon}$  model (Hwang and Lin, 1998), the individual components of the Reynolds stresses are determined in the framework of the isotropic representation:  $u' = v' = 2k/3$ . Satisfactory agreement between our simulations and the data of DNS predictions is obtained only when using the RSM approach.

The significant anisotropy of profiles velocity pulsations of a non-Newtonian fluid is obtained in predictions using RSM and ARSM, which is consistent with the data of (Singh et al., 2017) (see Table 1). The positions of the maxima in the distributions of axial and radial pulsations are in satisfactory agreement with the positions of the maxima for DNS (Singh et al., 2017). An exception is the distribution of radial fluctuations  $v'$  predicted using the isotropic  $k-\tilde{\varepsilon}$  model (Hwang and Lin, 1998) (see Table 2). The radial velocity fluctuations are significantly less than the intensity of axial fluctuations. The (Hwang and Lin, 1998) model describes well distribution of axial pulsation component along pipe radius (difference does not exceed 15%). In this case, there is a significant excess of radial fluctuations in comparison with the data [22] and our calculations using anisotropic turbulence models (Manceau and Hanjalic, 2002; Rokni, 2000) (up to 3 times).

The comparison of the DNS data (Singh et al., 2017) and our calculations of the axial velocity and kinetic energy of turbulence (KET) in wall units for the BS fluid are presented in Fig. 4. Here dots in Fig. 4b are the DNS data (Singh et al., 2017), curves are authors’ RANS calculation by using  $k-\tilde{\varepsilon}$  (Hwang and Lin, 1998), the RSM (Manceau and Hanjalic, 2002) and the ARSM (Rokni, 2000) turbulence models. Fig. 4a shows the velocity profiles  $U_+$  for NNF. Difference between the three turbulence models is insignificant in the regions ( $y_+ < 5$  and  $(5 < y_+ < 30)$ ). These results quantitative agree with the DNS data (Singh et al., 2017) (see Fig. 4a). Yield stress has practically no effect within the viscous sublayer and the differences between the various models are minimal. It qualitatively agrees with the conclusions of (Wilson and Thomas, 1985). For all three models, the difference is no more than 15% and the velocity profile is similar for a NF. Our RANS predictions and DNS at  $30 < y_+ < 200$  differ by up to 15%.

### 4.2. Turbulent non-isothermal flow structure

The distribution of the action zone of yield stress  $\tau_0/\tau_{NF} = 10$  along the axial coordinate depending on the ambient soil temperature is shown in Fig. 5. The zone height of yield stress  $\tau_0/\tau_{NF} = 10$

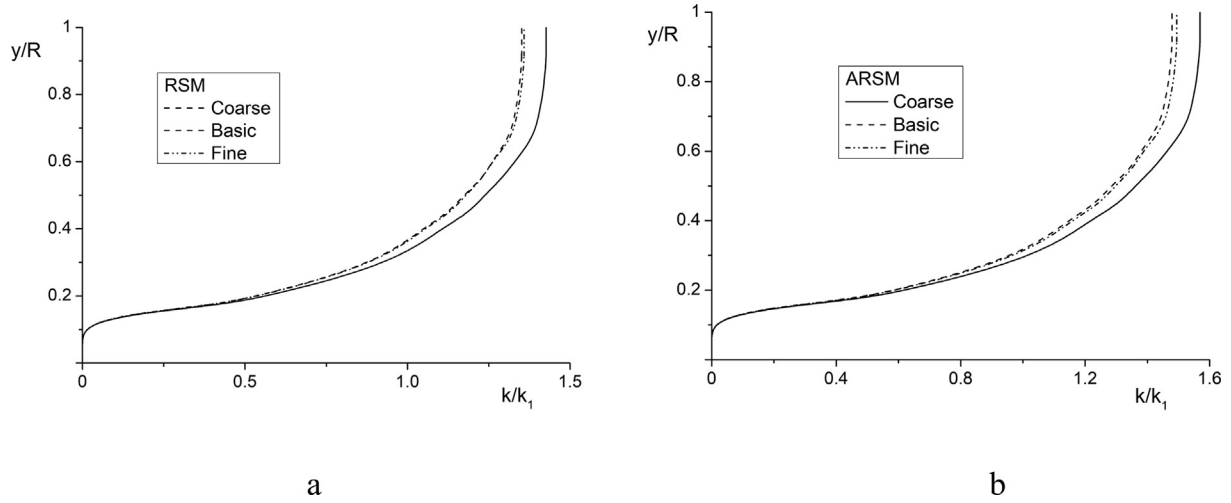


Fig. 2. The grid convergence test of "in-house" code for the RSM (a) and the ARSM (b).  $L = 2$  m,  $Re = 8200$ ,  $U_1 = 0.2$  m/s,  $T_1 = 298$  K,  $T_W = 273$  K.

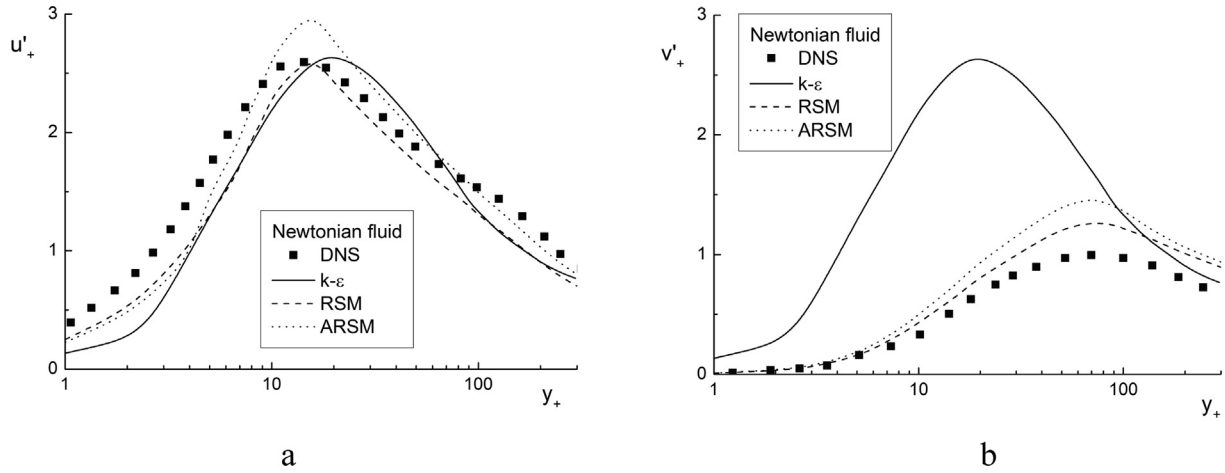


Fig. 3. Radial profiles of axial (a) and radial (b) velocities pulsations of a Newtonian fluid. Solid symbols are the DNS results (Singh et al., 2017) and lines are authors' RANS predictions. Solid lines are the  $k-\epsilon$  model (Hwang and Lin, 1998), dashed curves are the RSM (Manceau and Hanjalic, 2002) and dotted lines are the ARSM (Rokni, 2000).  $Re = 1.3 \times 10^4$ ,  $Re_\tau = 323$ .

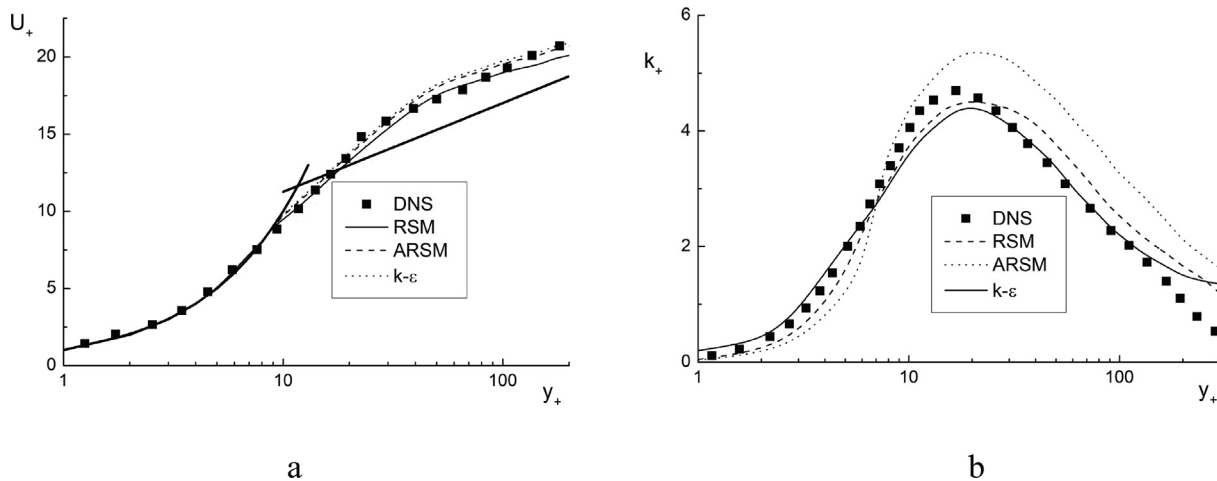


Fig. 4. Profiles of average axial velocity (a) and turbulent kinetic energy (b) of a NNF. Solid symbols are DNS results (Singh et al., 2017) and lines are authors' RANS predictions. Solid lines are the  $k-\epsilon$  model (Hwang and Lin, 1998), dashed curves are the RSM (Manceau and Hanjalic, 2002) and dotted lines are the ARSM (Rokni, 2000).  $Re = 1.3 \times 10^4$ ,  $Re_\tau = 323$ ,  $\tau_0/\tau_W = 1.2$ .

**Table 1**  
The positions of maximal values of the ratio of axial to radial velocities pulsations.

Reference	$(u'/v')_{max}$			
	$y_+ = 30$	$y_+ = 50$	$y_+ = 100$	$y_+ = 200$
DNS (Singh et al., 2017)	3.6	2.4	1.8	1.5
RSM (Manceau and Hanjalic, 2002)	2.8	2.1	1.6	1.35
ARSM (Rokni, 2000)	2.5	1.7	1.3	1.1

**Table 2**  
The transverse locations of maximal magnitudes of axial and radial velocities fluctuations.

Reference	$y_+(u'_{max})$	$y_+(v'_{max})$
DNS (Singh et al., 2017)	16	85
RSM (Manceau and Hanjalic, 2002)	17.5	90
ARSM (Rokni, 2000)	17	75
$k-\tilde{\epsilon}$ (Hwang and Lin, 1998)	20	20

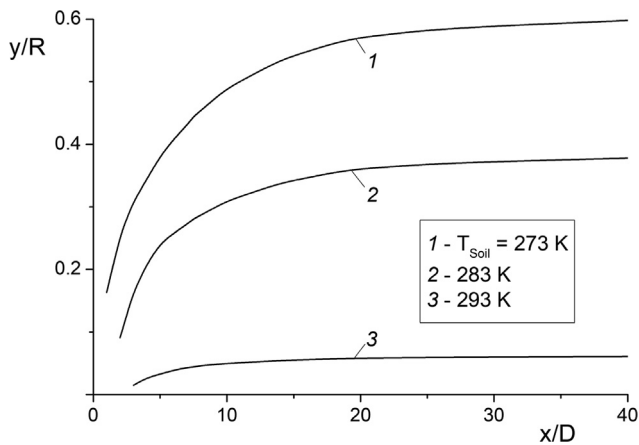


**Fig. 5.** Evolution of radial coordinates of yield stress values presence  $\tau_0/\tau_{NF} = 10$  along the pipe length.  $Re = 8200$ ,  $T_1 = 298$  K.

increases gradually along the streamwise coordinate. It tends to the coordinate  $y/R \approx 0.6$  at  $x/D = 40$  ( $x = 8$  m) for temperature  $T_S = 273$  K and  $y/R \approx 0.06$  for temperature  $T_S = 293$  K.

The effect of ambient soil temperature on the radial profiles of yield stress  $y/R$  is shown in Fig. 6. The viscoplastic non-Newtonian behavior of WCO is clearly shown at  $T_S = 273$  K. In this

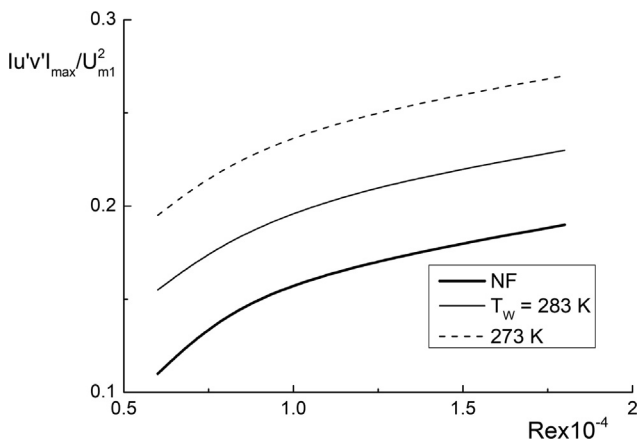


**Fig. 6.** Effect of Reynolds number on distributions of maximal values of the Reynolds stress.  $x/D = 20$ ,  $T_1 = 298$  K,  $T_{soil} = 273$  K.

case, the fluid with the manifestation of NNF properties occupies the most part of pipe cross-section ( $y/R \leq 0.75$ ). The yield stress value exceeds the stresses in a turbulent Newtonian fluid flow by several orders of magnitude. The magnitude of yield shear stress is minimal at  $T_S = 293$  K. The non-Newtonian behavior of waxy crude oil appears only in the pipe near-wall part ( $y/R \leq 0.2$ ).

### 4.3. Wall friction and heat transfer

In Fig. 7 distributions of wall friction and Nusselt numbers are represented at  $x/D = 10$ . Here wall friction coefficient is  $C_f = 2\tau_w/(\rho U_1^2)$  and the Nusselt number is  $Nu = hD/\lambda_w$ , heat transfer coefficient is  $h$ . Abbreviation FD is a fully developed Newtonian fluid and subscript  $W$  is a wall. The results are given in Fig. 7 are conducted for the developing flow of Newtonian waxy crude oil (NF line), and for the hydrodynamically fully developed Newtonian waxy crude oil (FD line). Therefore, the magnitude of heat transfer in the developing flow is higher than in the developed flow under all other conditions being equal. The coefficients of friction and heat transfer increase with an increase in the Reynolds number at the pipe inlet (see Fig. 7). It can be seen that the decrease in surrounding soil temperature causes a more rapid manifestation of the non-Newtonian properties of a Bingham-Schwedoff fluid and this confirms the conclusions from our previous predicted results. This leads to an increase in resistance (Fig. 7a) and a weakening of heat transfer (see Fig. 7b) of turbulent flow in pipe. Fluid velocity increase leads to a slow cooling of the turbulent flow, as well as an increase in the pipe length, where the Newtonian property of the fluid preserved.

The normalized distributions of wall friction  $C_f/C_{f,fd}$  (a) and heat transfer  $Nu/Nu_{fd}$  (b) on the wall during the turbulent fluid flow along streamwise coordinate are given in Fig. 8. A decrease in the environment temperature leads to a significant reduction in wall friction  $C_f$  and heat transfer  $Nu$ . Close to the wall, yield stress and a fluid stagnation zone appear (a medium behaves like a solid). The magnitudes of  $C_f$ ,  $Nu$  are equal to zero in this region. In the case of the manifestation of the yield stress in the near-wall region of the pipe, heat transfer is possible only due to thermal conductivity. It qualitatively agrees with the conclusions of (Aljerf, 2016; Aljerf and Al Masri, 2018).

### 5. Conclusion

A numerical RANS predictions of heat transfer of Bingham-Schwedoff fluid has been carried out. Fluid turbulence is described by the Reynolds stress model. A comparison is carried out with the DNS data predictions of a Bingham-Schwedoff isothermal turbulent fluid. The RSM agrees better with the DNS data on turbulent characteristics for an isothermal non-Newtonian Bingham-Schwedoff fluid than the ARSM and the  $k-\tilde{\epsilon}$  model.

Satisfactory agreement between our simulations and the DNS is obtained only using the RSM approach. The significant anisotropy of the profiles of velocity pulsations of a non-Newtonian fluid is obtained in predictions using the RSM and the ARSM. The aniso-

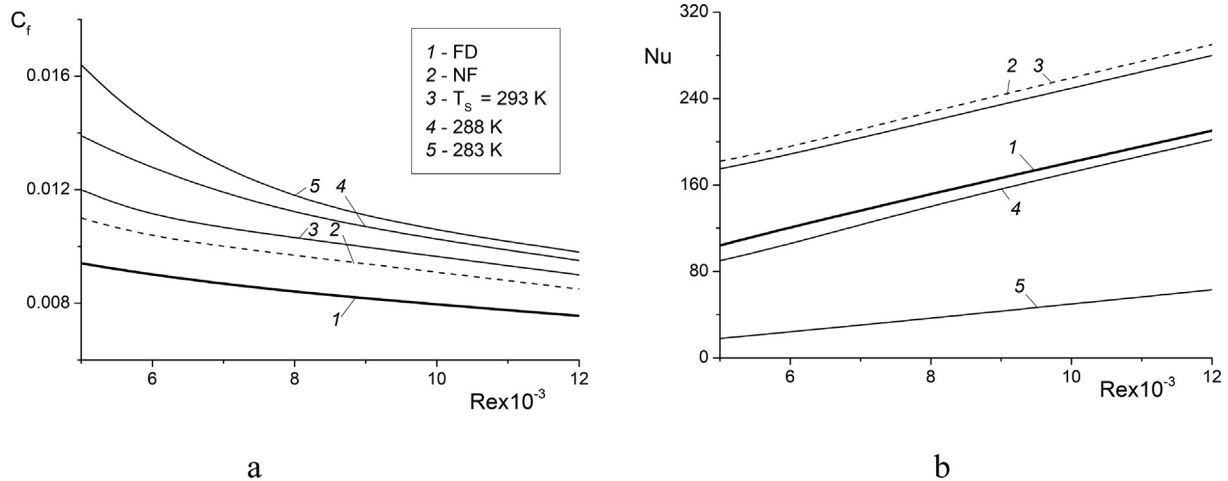


Fig. 7. Effect of Reynolds numbers on wall friction and Nusselt number at  $x/D = 10$ .

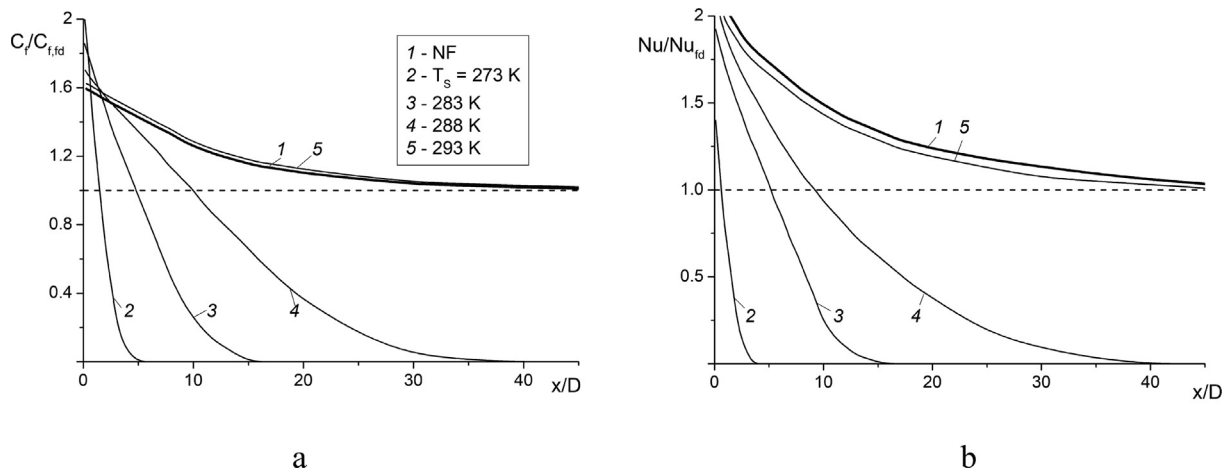


Fig. 8. Influence of soil temperature  $T_s$  on wall friction (a) and transfer (b) distributions of WCO along pipe length.  $Re = 8200$ ,  $T_1 = 298$  K.

tropy coefficient of pulsation velocities reaches  $AR = (u'/v')_{max} \approx 5.3$ . The shift of the locus of maximal values of turbulent pulsations, Reynolds stress, and turbulent kinetic energy towards the flow core is observed. In calculations, region of transition of Newtonian fluid to viscoplastic state is determined. An increase in fluid velocity leads to an increase in the pipe length, where Newtonian properties of fluid are preserved due to slower cooling of turbulent fluid flow.

The appearance of a non-Newtonian fluid property leads to an increase in resistance and a weakening of the heat transfer of a turbulent flow in the pipe. A decrease in surrounding environment temperature causes a significant decrease in the coefficient of wall friction and heat transfer due to the appearance of yield stress. The height of a stagnation zone of the fluid flow is numerically predicted. Close to the wall, yield stress and a fluid stagnation zone appear (a medium behaves like a solid). The magnitudes of  $C_f$ ,  $Nu$  are equal to zero in this region. Heat transfer in the case of manifestation of yield stress in near-wall region of pipe is possible only due to thermal conductivity.

**Declaration of Competing Interest**

The authors declare that they have no known competing financial interests or personal relationships that could have appeared to influence the work reported in this paper.

**Acknowledgements**

This work supported by the Science Committee of the Ministry of Science and Higher Education of the Republic of Kazakhstan (Grant number AP14869322 for 2022-2024).

**References**

Aiyejina, A., Chakrabarti, D.P., Pilgrim, A., Sastry, M.K.S., 2011. Wax formation in oil-pipelines: a critical review. *Int. J. Multiph. Flow* 37, 671–694.  
 Aljerf, L.M., 2016. Reduction of gas emission resulting from thermal ceramic manufacturing processes through development of industrial conditions. *Sci. J. King Faisal Univ.* 17 (1), 1–10.  
 Aljerf, L.M., Al Masri, M.N., 2018. Flame propagation model and combustion phenomena: observations, characteristics, investigations, technical indicators, and mechanisms. *J. Energy Conserv.* 1 (1), 31–40.  
 Anbarlooei, H.R., Cruz, D.O.A., Ramos, F., Santos, C.M.M., Silva Freire, A.P., 2017. Phenomenological friction equation for turbulent flow of Bingham fluids. *Phys. Rev. E* 96, 023107.  
 Barnes, H.A., 1999. The yield stress—a review or ‘παντα ρει’—everything flows? *J. Nonnewton. Fluid Mech.* 81, 133–178.  
 Bekibayev, T.T., Zhabbasbayev, U.K., Ramazanova, G.I., Minghat, A.D., Bosinov, D.Z., 2021. Simulation of oil pipeline shutdown and restart modes. *Complex Use Min. Resour.* 316, 15–23.  
 Bekibayev, T.T., Zhabbasbayev, U.K., Ramazanova, G.I., 2022. Optimal regimes of heavy oil transportation through a heated pipeline. *J. Process Control* 115, 27–35.  
 Beverly, C.R., Tanner, R.I., 1992. Numerical analysis of three-dimensional Bingham plastic flow. *J. Nonnewton. Fluid Mech.* 42, 85–115.

- Bingham, E.C., 1922. Fluidity and plasticity. McGraw-Hill, New York, U.S.A.
- Chhabra, R., Richardson, J., 2011. Non-Newtonian Flow and Applied Rheology: Engineering Applications. Butterworth-Heinemann, Oxford, U.K.
- Cruz, D.O.A., Pinho, F.T., 2003. Turbulent pipe flow predictions with a low Reynolds number k- $\epsilon$  model for drag reducing fluids. *J. Nonnewton. Fluid Mech.* 114, 109–148.
- Dai, Z.h., 2019. Analysis on influencing factors of buried hot oil pipeline. *Case Stud. Therm. Eng.* 16, 100558.
- De Oliveira, G.M., Vieira da Rocha, L., Franco Cezar, A.T., Negrão, O.R., 2010. Numerical simulation of the start-up of Bingham fluid flows in pipelines. *J. Non-Newt. Fluid Mech.* 165, 1114–1128.
- Durbin, P.A., Pettersson Reif, B.A., 2011. Reynolds Averaged Navier-Stokes Equations. Statistical Theory and Modeling for Turbulent Flows, 45–56. 2nd Edition, Chapter 3. John Wiley & Sons, Ltd, Chichester, U.K.
- Escudier, M.P., Nickson, A.K., Poole, R.J., 2009. Turbulent flow of viscoelastic shear-thinning liquids through a rectangular duct: Quantification of turbulence anisotropy. *J. Nonnewton. Fluid Mech.* 160, 2–10.
- Gnambode, P.S., Orlandi, P., Ould-Rouiss, M., Nicolas, X., 2015. Large-eddy simulation of turbulent pipe flow of power-law fluids. *Int. J. Heat Fluid Flow* 54, 196–210.
- Gavrilov, A.A., Rudyak, V.Y., 2016a. Direct numerical simulation of the turbulent flows of power-law fluids in a circular pipe. *Thermophys. Aeromech.* 23, 473–486.
- Gavrilov, A.A., Rudyak, V.Y., 2016b. Reynolds-averaged modeling of turbulent flows of power-law fluids. *J. Nonnewton. Fluid Mech.* 227, 45–55.
- Hwang, C.B., Lin, C.A., 1998. Improved low-Reynolds-number k- $\epsilon$  model based on direct simulation data. *AIAA J.* 36, 38–43.
- Iaccarino, G., Shaqfeh, E.S.G., Dubief, Y., 2010. Reynolds-averaged modeling of polymer drag reduction in turbulent flows. *J. Nonnewton. Fluid Mech.* 165, 376–384.
- Li, H., Zhang, J., Song, C., Sun, G., 2015. The influence of the heating temperature on the yield stress and pour point of waxy crude oils. *J. Pet. Sci. Eng.* 135, 476–483.
- Malin, M.R., 1997. The turbulent flow of Bingham plastic fluids in smooth circular tubes. *Int. Comm. Heat Mass Transfer* 24, 793–804.
- Manceau, R., Hanjalic, K., 2002. Elliptic blending model: a new near-wall Reynolds-stress turbulence closure. *Phys. Fluids* 14, 744–754.
- Masoudian, M., Pinho, F.T., Kim, K., Sureshkumar, R., 2016. A RANS model for heat transfer reduction in viscoelastic turbulent flow. *Int. J. Heat Mass Transf.* 100, 332–346.
- Masoumi, H., Aghighi, M.S., Ammar, A., 2019. Laminar natural convection of yield stress fluids in annular spaces between concentric cylinders. *Int. J. Heat Mass Transf.* 138, 1188–1198.
- Pakhomov, M.A., Zhabbasbayev, U.K., 2021. RANS modeling of turbulent flow and heat transfer of non-Newtonian viscoplastic fluid in a pipe. *Case Studies Therm. Eng.* 28, 101455.
- Papanastasiou, T.C., 1987. Flows of materials with yield. *J. Rheol.* 31, 385–404.
- Peixinho, J., Nouar, C., Desaubry, C., Théron, B., 2005. Laminar transitional and turbulent flow of yield stress fluid in a pipe. *J. Nonnewton. Fluid Mech.* 128, 172–184.
- Rokni, M., 2000. A new low-Reynolds version of an explicit algebraic stress model for turbulent convective heat transfer in ducts. *Num. Heat Transfer, pt B* 37, 331–363.
- Rudman, M., Blackburn, H.M., 2006. Direct numerical simulation of turbulent non-Newtonian flow using a spectral element method. *Appl. Math. Modelling* 30, 1229–1248.
- Salehi-Shabestari, A., Ahmadpour, A., Raisee, M., Sadegh, K., 2016. Flow and displacement of waxy crude oils in a homogenous porous medium: A numerical study. *J. Nonnewton. Fluid Mech.* 235, 47–63.
- Singh, J., Rudman, M., Blackburn, H.M., 2017. The effect of yield stress on pipe flow turbulence for generalised Newtonian fluids. *J. Nonnewton. Fluid Mech.* 249, 53–62.
- Speziale, C.G., Xu, X.H., 1996. Towards the development of second-order closure models for non-equilibrium turbulent flows. *Int. J. Heat Fluid Flow* 17, 238–244.
- Souas, F., Safri, A., Benmounah, A., 2021. A review on the rheology of heavy crude oil for pipeline transportation. *Petr. Res.* 6, 116–136.
- Vinay, G., Wachs, A., Agassant, J.-A., 2005. Numerical simulation of non-isothermal viscoplastic waxy crude oil flows. *J. Nonnewton. Fluid Mech.* 128, 144–162.
- Wilson, K.C., Thomas, A.D., 1985. A new analysis of the turbulent flow of non-Newtonian fluids. *Canadian J. Chem. Eng.* 63 (4), 539–546.
- Yigit, S., Hasslberger, J., Chakraborty, N., Klein, M., 2020. Effects of Rayleigh-Bénard convection on spectra of viscoplastic fluids. *Int. J. Heat Mass Transf.* 147, 118947.
- Zhabbasbayev, U.K., Ramazanova, G.I., Bossinov, D.Z., Kenzhaliyev, B.K., 2021. Flow and heat exchange calculation of waxy oil in the industrial pipeline. *Case Stud. Thermal Eng.* 26, 101007.
- Zhumagulov, B.T., Smagulov, S.S., Evseeva, A.U., Nesterenkova, L.A., 2002. Pipeline transportation of highly viscous and highly solidifying oils. *Gylm, Almaty, Kazakhstan.*